Hybrid Characterization of Nanolitre Dielectric Fluids in a Single Microfluidic Channel Up to 110 GHz

Song Liu, Nathan D. Orloff, Charles A. E. Little, Wei Zhao, James C. Booth, Dylan F. Williams, *Fellow, IEEE*, Ilja Ocket, *Member, IEEE*, Dominique M. M.-P. Schreurs, *Fellow, IEEE*, and Bart Nauwelaers, *Senior Member, IEEE*

***Abstract*— In this paper, we present a new "hybrid" method for on-wafer dielectric measurements of nanolitre fluid samples. The first part of the hybrid method uses a technique that extracts the complex relative permittivity of the material used to make microfluidic channels. The extraction is performed with an empty channel measurement, and thus requires no extra deembedding structures. The second part of the hybrid method involves an accurate extraction of the complex relative permittivity of dielectric fluids. The hybrid method uses three different extraction algorithms and calculates their Type B uncertainties within the NIST Microwave Uncertainty Framework. By choosing the calculation algorithm with the smallest uncertainty at each frequency, the hybrid method can achieve accurate measurements of the fluids' permittivity over a broad bandwidth. One of the three algorithms is a new algorithm based on closed-form equations. A trace-based algorithm is also applied to fluids measurements, for the first time to our knowledge. Through the uncertainty analysis, we found out that these two algorithms should be favored over a traditional least-squares optimization-based algorithm at millimeter wave frequencies, due to their lower sensitivities to probe-placement errors.**

***Index Terms*— Dielectric liquids, microfluidics, millimeter wave technology.**

I. Introduction

DIELECTRIC spectroscopy of liquids between 1 MHz and 110 GHz is a valuable tool for studying chemical and biological structures on the microscopic level. In [1], the molecular structures in alcohol–water mixtures were investigated through measurements of their multimodal GHz dielectric relaxations. Reference [2] has shown correlations between the water relaxations around 20 GHz in protein solutions and protein shapes, while the intrinsic dielectric relaxations of protein molecules lie in the megahertz region [3]. In [4], protein hydration number, i.e., the number of tightly-bound water molecules per protein, was calculated from the weak megahertz protein bound water relaxation. Reference [5] also shows protein hydration studies by millimeter wave and terahertz dielectric spectroscopy. For cells suspensions, the megahertz relaxations are directly related to the cell sizes and the membrane unit capacitance, which has been shown by the Pauly and Schwan model [6], [7].

The combination of microfluidics technology and microwave techniques is gaining interest these years because of the promising applications. The downscaling of liquid volumes offered by microfluidics allows dielectric fluids sensing [8], [9] and metrology [10] to be performed with nanolitre fluid volumes, which is especially interesting for measurements of precious samples. Single-cell techniques from microfluidics are being used by researchers to perform dielectric spectroscopy with a much higher level of specificity and sensitivity compared with bulk suspensions measurements [11], [12].

Coplanar waveguide (CPW) transmission lines are getting more popular as sensing electrodes for low-volume measurements of dielectric fluids' permittivity [8], [10], [13]–[15] due to their confined fields in the slots, ease of fabrication, and ease of integration with fluidic structures. Other methods have been successfully developed for dielectric fluids measurements, e.g., the traveling-wave method [16], the free-space method [17], the waveguide-interferometer method [18], and the popular dielectric probe method [19], [20]. However, these methods are not readily integratable with microfluidics structures, which are mostly planar [21], [22].

In this paper, we will focus on quantitative complex permittivity measurements of dielectric fluids with CPW microfluidic structures. For CPW microfluidic measurements, the impact of the microfluidic channel walls must be removed from the microwave measurements, so that the dielectric fluids' permittivity can be extracted. There are a number of ways to accomplish this deembedding step. In the least-squares optimization-based method [10], the microfluidic device was modeled as sections of cascaded uniform transmission lines.

Manuscript received February 1, 2017; revised June 11, 2017; accepted July 1, 2017. Date of publication August 8, 2017; date of current version December 12, 2017. This work was supported in part by the Flemish Fund for Scientific Research (FWO), in part by the ARFTG 2013 Student Fellowship, and in part by the MTT-S 2014 Graduate Fellowship. The work of S. Liu was supported by the Junior Mobility Program in KU Leuven, Belgium, for the Travel Grant. *(Corresponding author: Song Liu.)*

S. Liu, D. M. M.-P. Schreurs, and B. Nauwelaers are with the ESAT-TELEMIC Division, KU Leuven, 3001 Leuven, Belgium (e-mail: song.liu3000@gmail.com).

N. D. Orloff, J. C. Booth, and D. F. Williams are with the National Institute of Standards and Technology (NIST), Boulder, CO 80305 USA (e-mail: booth@boulder.nist.gov).

C. A. E. Little is with the National Institute of Standards and Technology (NIST), Boulder, CO 80305 USA, and also with the University of Colorado Boulder, Boulder, CO 80309 USA (e-mail: cully.little@boulder.nist.gov).

W. Zhao is with the School of Electro-Mechanical Engineering, Xidian University, Xi'an 710126, China (e-mail: weizhao.xidian@gmail.com).

I. Ocket is with imec, 3001 Heverlee, Belgium, and also with the ESAT-TELEMIC Division, KU Leuven, 3001 Leuven, Belgium (e-mail: ilja.ocket@imec.be).

Color versions of one or more of the figures in this paper are available online at http://ieeexplore.ieee.org.

Digital Object Identifier 10.1109/TMTT.2017.2731950

By measuring extra microfluidic devices with zero channel length, the characteristics of the different transmission line sections were obtained. This method is broadband and accurate, but at the cost of fabricating and measuring extra structures. The reference device technique in the literature [8], [23], [24] also makes use of a microfluidic device with a zero-length microfluidic channel, which is the reference device. In the reference device technique, fluid properties are extracted from the measured difference between the fluid-filled device and the reference device without fluid samples. The extraction routine is simple and does not require a model of the transition from the probe tip to the microfluidic channel. Despite its simplicity, the reference device technique is inaccurate at low frequencies, due to the decreased difference in S-parameters between the fluid-filled device and the reference device.

Without requiring any reference devices, our recently developed calibration fluid method enables the deembedding to the microfluidic channel with a single device and two calibration liquids with unknown permittivities [25]. However, like the previous reference device technique, it relies on relative measurements. As a result, it is also inaccurate at low frequencies where the differences between the calibration measurements are inadequate.

In this paper, we propose a hybrid method for dielectric fluids measurements using a single CPW microfluidic device and over a wide bandwidth. Using the hybrid method, we can first use a new technique that is capable of measuring the broadband complex permittivity of the material used to make the microfluidic channel. The hybrid method then calculates the complex permittivity of dielectric fluids from three independent algorithms and evaluates their measurement uncertainties within the NIST Microwave Uncertainty Framework [26]. The three algorithms are the traditional least-squares optimization-based algorithm [10], a closed-form equation-based algorithm, and a trace-based algorithm [27]. By selecting one of the three algorithms with the smallest uncertainty at each frequency, the hybrid method can achieve accurate measurements of dielectric fluids' permittivity over a broad bandwidth.

We validated the hybrid method by measurements of deionized water at 22 °C. We performed the uncertainty analysis in a Type B fashion, where estimates of the effects of the error sources are derived from prior knowledge of the error sources instead of from repeated measurements [28]. We will show that the least-squares optimization-based algorithm was most accurate at low frequencies. However, we found that our measurements were increasingly sensitive to probe-placement errors at millimeter-wave frequencies, where the other two algorithms were less sensitive.

In this paper, we first introduce the hybrid method. We then discuss the measurement setup and fabrication. After that, we explain the method of uncertainty analysis and present measurement results of microfluidic channel wall material characterization. Next, we illustrate the hybrid method with deionized water at 22 °C as an example. We also show in detail the uncertainty analysis for water permittivity extraction. Finally, some conclusions are drawn.

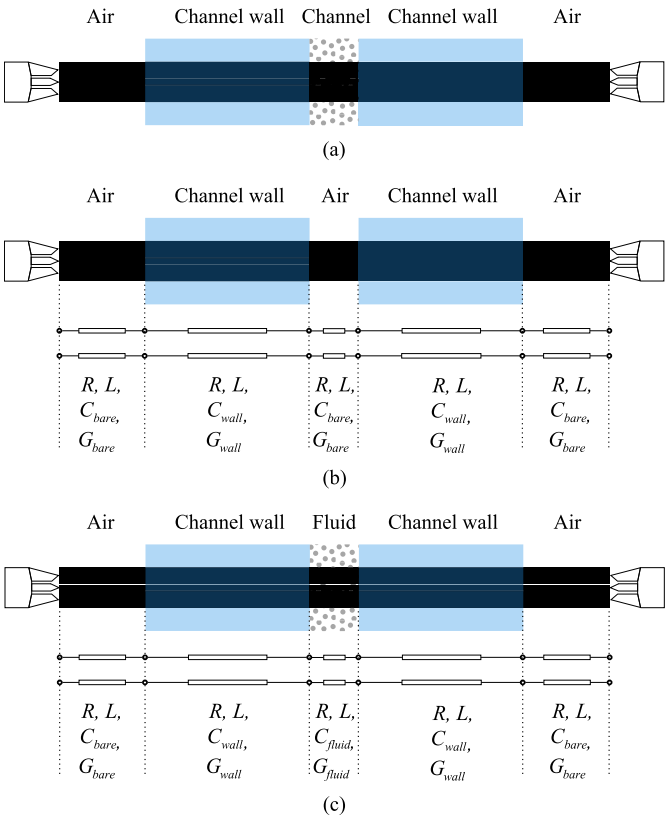

Fig. 1. Schematic of CPW microfluidic devices. (a) General schematic of a CPW microfluidic device. (b) Model of the CPW microfluidic device when it is empty. Different regions along the CPW line are modeled by distributed transmission line parameters R, L, C, and G. (c) Model of the CPW microfluidic device when the microfluidic channel is filled with fluid.

II. Hybrid Method for Dielectric Fluids Characterization

A. Introduction to the Hybrid Method

In this section, we explain the hybrid method for dielectric fluids characterization. Fig. 1(a) shows a general schematic of a CPW microfluidic device for dielectric fluids characterization. The CPW electrodes are usually realized on low-loss substrates. The CPW line has a uniform cross section along its length and is covered by different materials, i.e., air, the material used to make the microfluidic channel, and the dielectric fluid in the channel. The hybrid method is based on deembedding up to the inside of the microfluidic channel. For this reason, a method for characterizing the microfluidic channel wall material is introduced.

The proposed channel wall characterization method only uses an empty channel measurement and a set of multiline TRL (MTRL) calibration [29] standards realized on the same microfluidic wafer. Fig. 1(b) shows the model of the CPW microfluidic device for the empty channel case. The microfluidic device is modeled by a cascade of transmission line sections characterized by the resistance R, the inductance L, the capacitance C, and the conductance G per unit length. C and G of the bare transmission lines are called C_{bare} and G_{bare}, respectively. C and G of the transmission lines covered with the channel wall material are called

C_{wall} and G_{wall}, respectively. The empty microfluidic channel can be approximated by a section of bare transmission line, provided that the channel height is several times the CPW gap width. Since this paper deals with dielectric fluids, all the transmission line sections have the same resistance and inductance per unit length. C_{wall} and G_{wall} can be determined by taking advantage of the redundancy in the measurements.

From the measured C_{wall} and G_{wall}, 2-D finite-element simulations can be used to determine the complex relative permittivity of the microfluidic channel wall material. In this paper, Ansys' Q3D[1] is used to perform the 2-D simulations. This simulation-based approach has been used previously to determine another material used to make the microfluidic channel: polydimethylsiloxane (PDMS) [10].

Fig. 1(c) shows the model for the fluid-filled channel case. In this case, C and G of the fluid-filled channel are denoted as C_{fluid} and G_{fluid}. The hybrid method makes use of three permittivity-extraction algorithms that calculate C_{fluid} and G_{fluid} in different manners. Similar to the channel wall material characterization, the complex relative permittivity ($\epsilon_r = \epsilon_r' - j\epsilon_r''$) of the dielectric fluid under test is inverted from C_{fluid} and G_{fluid} by running 2-D simulations of the CPW cross section [10].

In the 2-D simulations, the real part of the complex relative permittivity of the material covering the CPW line $\epsilon_{r,\text{test}}'$ is swept from 1 to 101 in 21 steps, and the imaginary part of the complex relative permittivity $\epsilon_{r,\text{test}}''$ is set close to zero. From each simulation, the capacitance per unit length $C_{\text{unit,test}}$ is extracted. From the $C_{\text{unit,test}}$ - $\epsilon_{r,\text{test}}'$ table, the cross-sectional geometry-dependent linear coefficient linking $\epsilon_{r,\text{test}}'$ and $C_{\text{unit,test}}$ is extracted. The same coefficient links the imaginary part of the complex relative permittivity to the conductance per unit length divided by the angular frequency. This linear coefficient is used to invert ϵ_r from C_{fluid} and G_{fluid}.

At each frequency, the NIST Microwave Uncertainty Framework calculates the uncertainties in the extracted complex relative permittivity from the different extraction algorithms. The uncertainty calculation includes both the uncertainties in the on-wafer MTRL calibration and in the on-wafer microfluidic measurement. After the uncertainty calculation, the hybrid method selects the algorithm with the smallest uncertainty at each frequency. In this way, the complex relative permittivity of fluid can be extracted with high accuracy over a wide bandwidth. In what follows, the method for characterizing the material used to make the microfluidic channel and the three permittivity extraction algorithms are explained in detail.

B. Single-Length Method for Characterizing the Material Used to Make the Microfluidic Channel

Since the hybrid method for dielectric fluids characterization relies on the S-parameters of the transmission line section covered with dielectric fluids [Fig. 1(c)], the reference plane has to be translated to the inside of the channel. For this purpose, we use an on-wafer MTRL calibration to correct the vector network analyzer (VNA) to the probe tips.

1) Bare Line Characterization: The reference impedance of the MTRL calibration can be determined through the propagation constant and the measured capacitance per unit length C_{bare} [30]. Since the microfluidic substrate is usually low loss and nondispersive, we can determine C_{bare} following the method of Williams [31] and set G_{bare} to zero. After that, R and L can be determined by the following simple relationship [30]:

$$R + j\omega L = \frac{\gamma^2}{j\omega C_{\text{bare}}} \tag{1}$$

where γ is the measured propagation constant of the bare lines from the MTRL calibration. After the MTRL calibration and the bare line characterization, the reference plane can be translated to the outside of the microfluidic channel with a 50-Ω reference impedance.

2) Microfluidic Channel Characterization: The microfluidic channel wall material can be characterized by taking advantage of the redundancy in the measurements. From Fig. 1(b), we see that only C_{wall} and G_{wall} are unknown. The measured S-parameters of the empty channel have eight independent real numbers if the device is asymmetrical, and four independent real numbers if the device is symmetrical. In both cases, the number of knowns is greater than the number of unknowns, making the unknowns overdetermined. A least-squares optimization method can be used to solve C_{wall} and G_{wall} from the measured empty channel S-parameters. After this step, the reference plane can be translated to the inside of the microfluidic channel, so the S-parameters of the fluid-covered CPW line are available for permittivity extraction of the fluid sample under test.

C. Dielectric Fluids Characterization Algorithms

Three algorithms are used by the hybrid method to calculate the fluid's relative permittivity from the measured S-parameters of the fluid-covered CPW line. These algorithms extract C_{fluid} and G_{fluid} in different ways. Because different algorithms are suitable for different frequency bands, they are all required for the hybrid method to achieve accurate measurements over the widest possible bandwidth.

1) Least-Squares Optimization: The first algorithm is based on least-squares optimizations and has previously been reported in [10]. From the estimated capacitance $C_{\text{fluid,est}}$ and conductance $G_{\text{fluid,est}}$ per unit length and measured R and L, the S-parameters of the fluid-covered CPW line can be modeled. The algorithm finds the optimal $C_{\text{fluid,est}}$ and $G_{\text{fluid,est}}$ that minimize the least-squares errors between the measured and modeled S-parameters. As will be shown by the measurements in Section V, this algorithm, in comparison to the other approaches explored here, had lower uncertainties and agreed more closely with the accepted literature values at low frequencies.

2) Closed-Form Equations: The second algorithm is based on closed-form equations. First, the measured S-parameters of the fluid-covered CPW line are converted to the *ABCD*

[1]NIST does not endorse commercial products. Product information is given only to describe the procedure. Other products may work as well or better.

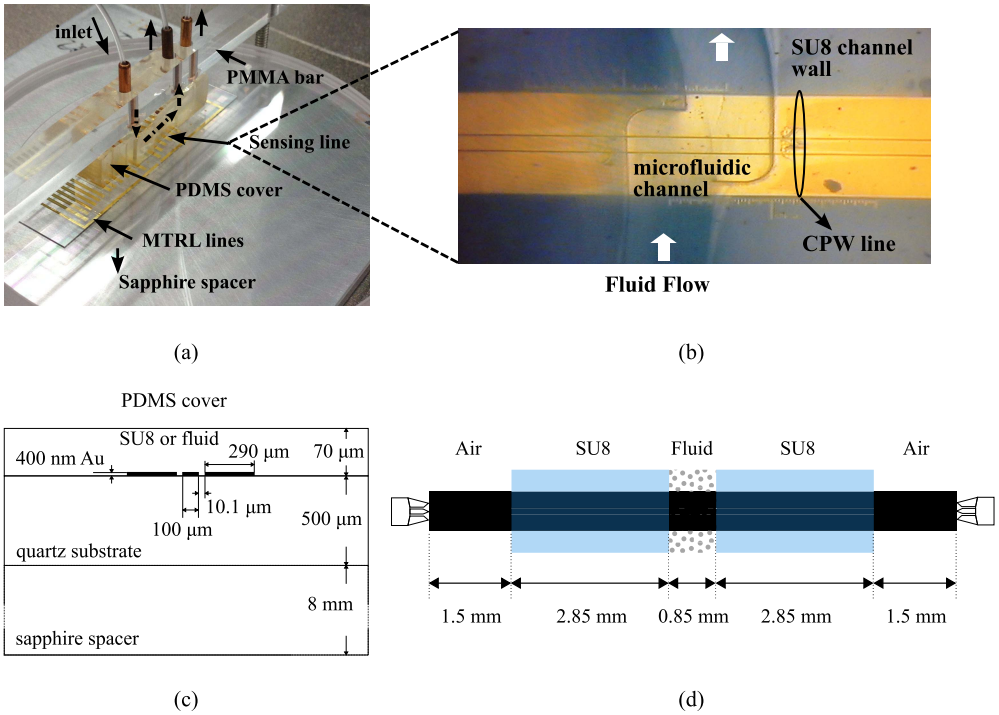

Fig. 2. (a) Microfluidic measurement setup. The dashed lines indicate the fluid flow. (b) Microphotograph of the microfluidic channel. (c) Cross-sectional dimensions of the CPW transmission line of the SU8 region or the fluid region. The SU8 region and the fluid region are defined in (d). (d) Lengths of different regions on the CPW transmission line.

matrix form [32]. The *ABCD* matrix is related to the propagation constant γ_{fluid} and the characteristic impedance $Z_{c,\text{fluid}}$ by the following equation:

$$\begin{bmatrix} A & B \\ C & D \end{bmatrix} = \begin{bmatrix} \cosh(\gamma_{\text{fluid}} l) & Z_{c,\text{fluid}} \sinh(\gamma_{\text{fluid}} l) \\ \dfrac{1}{Z_{c,\text{fluid}}} \sinh(\gamma_{\text{fluid}} l) & \cosh(\gamma_{\text{fluid}} l) \end{bmatrix} \tag{2}$$

where l is the length of the microfluidic channel. From this overdetermined system of equations, we can extract the propagation constant ($\gamma_{\text{fluid}} = \alpha + j\beta$) with the following closed-form equations:

$$E = e^{\gamma_{\text{fluid}} l} = \sqrt{BC} + \frac{A + D}{2} \tag{3a}$$

$$\alpha = \frac{\ln(|E|)}{l} \tag{3b}$$

$$\beta = \frac{\angle E}{l}. \tag{3c}$$

C_{fluid} and G_{fluid} can be extracted from γ_{fluid} from this simple relationship

$$j\omega C_{\text{fluid}} + G_{\text{fluid}} = \frac{\gamma_{\text{fluid}}^2}{j\omega L + R}. \tag{4}$$

The measurements will show that this algorithm was accurate at high frequencies.

3) Trace: The third algorithm is based on the matrix trace of a difference matrix. Suppose the measured switch-term corrected [33] wave-cascading matrix of the empty channel and the fluid-filled channel are called M_{empty} and M_{fluid}, respectively. Here, M_{empty} and M_{fluid} can be calibrated or uncalibrated wave-cascading matrices. Since the resistance and the inductance per unit length of the empty channel and the fluid-filled channel are the same, their propagation constants γ_{empty} and γ_{fluid}, and the matrix trace of $M_{\text{fluid}} M_{\text{empty}}^{-1}$ are related by the following equation [27]:

$$\begin{aligned} Tr[M_{\text{fluid}} M_{\text{empty}}^{-1}] &= 2\cosh(\gamma_{\text{fluid}} l)\cosh(\gamma_{\text{empty}} l) \\ &\quad - \left(\frac{\gamma_{\text{fluid}}}{\gamma_{\text{empty}}} + \frac{\gamma_{\text{empty}}}{\gamma_{\text{fluid}}}\right) \sinh(\gamma_{\text{fluid}} l) \sinh(\gamma_{\text{empty}} l). \end{aligned} \tag{5}$$

In practice, the empty channel can be approximated by a piece of bare line, so in (5), γ_{empty} can be replaced by γ_{bare}. From (5), γ_{fluid} can be extracted by a least-squares optimization program.

This trace algorithm was initially developed for coaxial measurement of PDMS [27]. Here, we demonstrate its application to on-wafer fluid measurements. Since the trace method relies on the difference between two measurements, we found that it was better suited for high frequencies. A similar eigenvalue-based technique proposed by Janezic and Jargon [34] and later used by Grenier *et al.* [8], Meyne *et al.* [23], [24], and Huynen *et al.* [35] also extracts the propagation constant from relative measurements, but it requires an extra zero-length channel.

III. Microfluidic Measurement Setup and Fabrication

Fig. 2(a) shows the microfluidic measurement setup. The microfluidic device used in our experiments was a quartz wafer with gold CPW-sensing electrodes and SU8 microfluidic channels. SU8 is a negative, epoxy-type, near-UV

photoresist, which was developed for ultrathick high-aspect-ratio MEMS-type applications [36]. Fig. 2(b) shows a magnified view of the microfluidic channel. Fig. 2(d) shows the lengths of different regions with the sensing electrodes and Fig. 2(c) shows the cross-sectional geometry of the CPW-sensing electrodes. The conductor thickness and the CPW gap width were measured with a profilometer. The volume of fluid in the sensing region is about 40 nL.

The SU8 channels were sealed by a PDMS cover, which was clamped onto the microfluidic wafer by an acrylic glass (PMMA) bar. PDMS is gas permeable, so it helps the removal of air bubbles during the microfluidic measurements. On the same microfluidic wafer, we fabricated an on-wafer MTRL calibration kit. The CPW calibration lines had the same cross-sectional geometry as the CPW sensing electrodes. Their lengths were 9.2 (thru), 4.6 (short), 9.55, 10.25, and 11.835 mm. The quartz microfluidic wafer with the CPW lines and the SU8 channels on one side was placed on 8 mm of sapphire spacers to reduce the coupling to the parasitic microstrip mode between the CPW conductors and the metal holder.

The CPW electrodes were lithographically defined on the quartz substrate and fabricated with a liftoff technique [37]. The CPW conductors were formed by the first electron beam evaporating about 20-nm-thick titanium adhesion layer and then around 350-nm-thick gold layer. The measured metal thickness after fabrication was around 400 nm. After evaporating the gold layer, 70-μm-thick SU8 was spin coated on the quartz substrate. The SU8-coated quartz substrate was then soft-baked and exposed through a photomask on a contact aligner. After a postexposure bake, the final SU8 channel was formed and the SU8 thickness was measured to be around 70 μm. The microfluidic channels fabricated using the SU8 process were aligned to within 1 μm of the intended position, which was more accurate than our previous work [10].

Measurements were performed with the measurement setup discussed in this section at room temperature (22 °C). S-parameters from 0.1 to 110 GHz in logarithmic steps were measured for the MTRL calibration structures, empty microfluidic channel, and the fluid-filled microfluidic channel. Deionized water at 22 °C was used to validate the hybrid method, because the permittivity of biological fluids, e.g., protein solutions [2] and cell suspensions [15], is close to that of water. First, we present the measurement results of the material used to make the microfluidic channel, SU8. After that, the measurement results of deionized water at 22 °C are presented, followed by an uncertainty analysis of the different extraction algorithms.

IV. Uncertainty Analysis Method and Measurement Results of SU8

A. Method of Uncertainty Analysis

The hybrid method makes a selection among the different permittivity extraction algorithms (Section II-C) based on their measurement uncertainties. The NIST Microwave Uncertainty Framework was used to assess the uncertainties in the MTRL calibration and in the on-wafer microfluidic measurements. Table I lists the error mechanisms used for the uncertainty analysis. Error mechanisms in the MTRL calibration are shown in Table I (top). Uncertainties in the conductor thickness, cross-sectional dimensions, and contact resistances were obtained from repeated geometrical measurements. We estimated the uncertainty in the line lengths at 0.5 μm, which was based on the projection lithography tool that we used to pattern the devices. Since there were probe alignment markers spaced 10 μm from each other next to the CPW lines, the probe-placement error was estimated to be 5 μm. The variability in conductivity between different CPW lines used for the MTRL calibration was estimated to be 0.1% based on typical cleanroom fabrication capability.

For the uncertainty in the capacitance per unit length, 0.01 pF/cm (nominal value is 1.045 pF/cm) was used, because the capacitance per unit length was measured with high accuracy following the series-resistor technique [38]. Similar estimates were taken for the error mechanisms in the microfluidic channel measurements, which are shown in Table I (bottom). In this uncertainty analysis, linear propagation of uncertainties was assumed. When propagating uncertainties in C_{fluid} and G_{fluid} to ϵ_r, the linear coefficient used to invert ϵ_r from C_{fluid} and G_{fluid} is assumed constant.

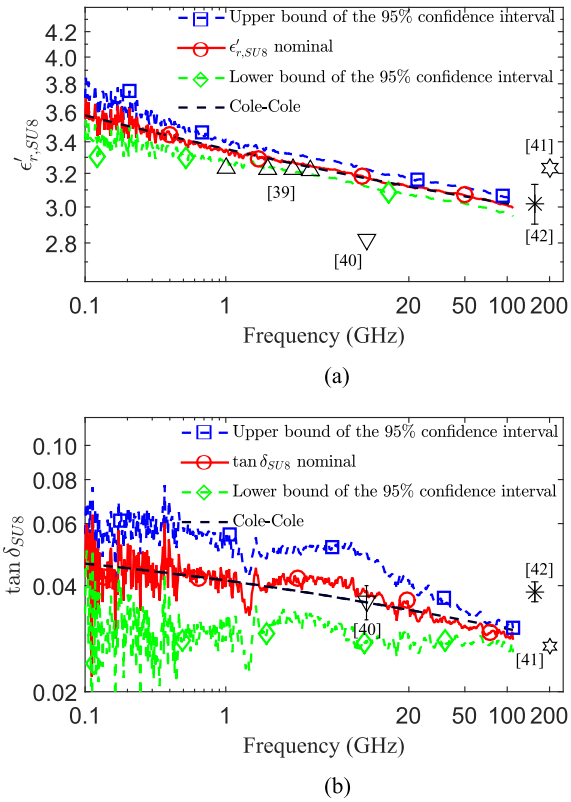

Fig. 3. Measured SU8 (a) relative permittivity and (b) loss tangent together with the literature values [39]–[42].

B. Measurement Results for SU8

Fig. 3 shows the measured real part of the complex relative permittivity $\epsilon'_{r,\text{SU8}}$ and the loss tangent $\tan\delta_{\text{SU8}}$ for SU8

TABLE I
TABLE OF ERROR MECHANISMS FOR UNCERTAINTY ANALYSIS

Error mechanisms in the multiline TRL calibration				
Error mechanism	unit	nominal value		estimated standard uncertainty
Conductor thickness	nm	400		10
Probe-placement	μm	0		5
CPW cross-section	μm	center conductor	100	0.067
	μm	slot width	10.10	0.047
	μm	ground plane width	290	0.047
CPW line length	μm	Line 1	9200	0.5
	μm	Line 2	9550	0.5
	μm	Line 3	10250	0.5
	μm	Line 4	11835	0.5
	μm	Short	4600	0.35
Conductivity	S/m	3.5e7		3.5e4
CPW line capacitance	pF/cm	1.045		0.01
Contact resistance	mΩ	0		52.35
Error mechanisms in the microfluid channel				
Error mechanism	unit	nominal value		estimated standard uncertainty
Probe-placement	μm	0		5
Contact resistance	mΩ	0		52.35
Microfluidic channel length	μm	total length	9550	0.5
	μm	left air section	1500	0.35
	μm	right air section	1500	0.35
	μm	left SU8 section	2850	0.35
	μm	right SU8 section	2850	0.35

from 0.1 to 110 GHz. Our measured values agree well with the literature values [39]–[42]. The differences might be due to the difference in SU8 batches, the curing processes, or even the measurement uncertainties associated with the different methods in the literature. The measured complex relative permittivity of SU8 was fit with a Cole–Cole relaxation model due to the distributed relaxation of SU8. The Cole–Cole relaxation model is described as follows:

$$\epsilon_r = \epsilon_\infty + \frac{\epsilon_s - \epsilon_\infty}{1 + j\omega\tau^{1-\alpha}} \tag{6}$$

where ϵ_r is the complex relative permittivity, ϵ_∞ and ϵ_s are the relative permittivity at infinitely high frequencies and at dc, respectively, τ is the dielectric relaxation time constant, and α describes the broadening of the dielectric relaxation. The relaxation frequency is related to the relaxation time constant via

$$f_r = \frac{1}{2\pi\tau}. \tag{7}$$

The fit Cole–Cole model parameters are listed in Table II. From the Cole–Cole parameters, we conclude that SU8 has a broadly distributed relaxation around 9.1 kHz. Because the measurement frequency range was far above the SU8 relaxation frequency, the 95% confidence intervals (CIs) of some of the relaxation parameters, ϵ_s and τ, are wide. More accurate measurements of SU8 permittivity at low frequencies and the relaxation parameters ϵ_s and τ could be obtained by using series-capacitor devices [43].

TABLE II
COLE–COLE RELAXATION PARAMETERS OF SU8 AND 95% CIS OF THE RELAXATION PARAMETERS FROM FITTING THE NOMINAL SU8 RELATIVE PERMITTIVITY

	ϵ_∞	ϵ_s	τ (us)	α
Cole-Cole	2.52	7.11	17.45	0.872
95% CI	2.36 – 2.68	3.16 – 11.05	-171 – 206	0.827 – 0.917

V. MEASUREMENT RESULTS OF DEIONIZED WATER AT 22 °C

In this paper, u denotes the uncertainty of the measured relative permittivity and u % denotes the relative uncertainty of the permittivity in percentage. Fig. 4(a) and (b) shows the uncertainties of the measured real and imaginary parts of the complex relative permittivity of water for the different algorithms mentioned in Section II-C and the hybrid method. In Fig. 4(a) and (b), $u(\epsilon_{r,\mathrm{H_2O,lsq}})$, $u(\epsilon_{r,\mathrm{H_2O,cf}})$, and $u(\epsilon_{r,\mathrm{H_2O,trace}})$ denote the uncertainties in the complex relative permittivity obtained with the least-squares optimization algorithm, the closed-form equations algorithm, and the trace algorithm, respectively, and $u(\epsilon_{r,H_2O,\mathrm{hybrid}})$ denotes the uncertainties of the hybrid method.

The least-squares optimization algorithm shows the smallest uncertainties at low frequencies, but its uncertainties increase at high frequencies. The closed-form equation algorithm and the trace algorithm show much higher uncertainties than the least-squares optimization algorithm at low frequencies,

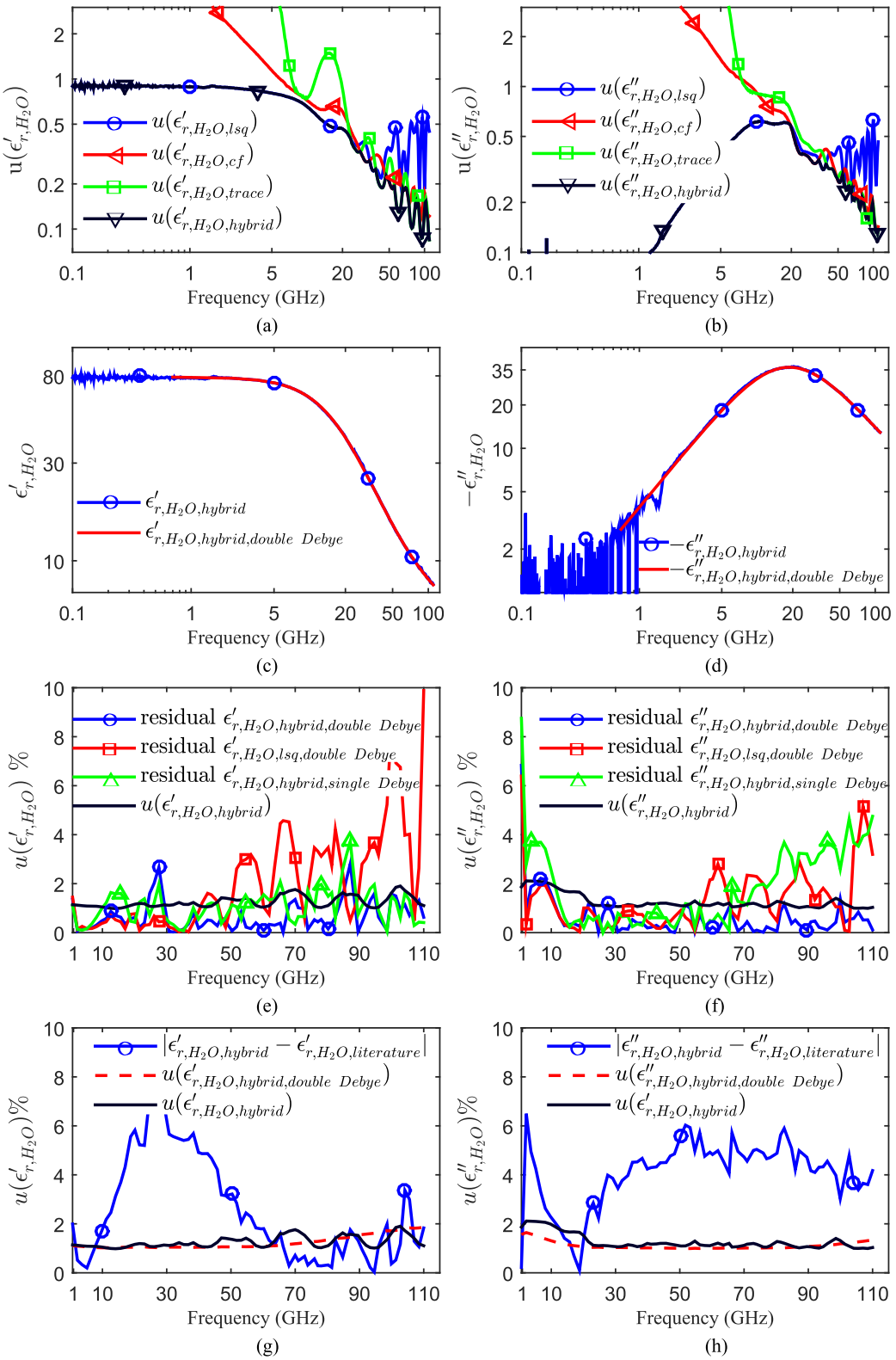

Fig. 4. Extracted complex relative permittivity of deionized water at 22 °C using the hybrid method. Uncertainties in the measured (a) real and (b) imaginary parts of the complex relative permittivity using the different algorithms. (c) Real and (d) imaginary parts of the complex relative permittivity measured with the hybrid method $\epsilon_{r,\mathrm{H_2O,hybrid}}$ and the fitting of the hybrid data to a double Debye model $\epsilon_{r,\mathrm{H_2O,hybrid,double\ Debye}}$ (8). (e) Real and (f) imaginary parts of the fitting residuals in percentage. The fittings were performed with the measured relative permittivity from the least-squares optimization algorithm or the hybrid method, and the fitting model was either the single Debye model or the double Debye model. (g) Real and (h) imaginary parts of the difference between the measured complex relative permittivity of water and the literature values [44] in percentage.

but have lower uncertainties at high frequencies. The reasons for the frequency-dependent characteristics of the uncertainties will be addressed in Section VI. The hybrid method selected the permittivity extraction algorithm with the smallest uncertainty at each frequency, so its curves coincide with the extraction algorithm with the smallest uncertainty.

TABLE III
MEASURED DOUBLE-DEBYE RELAXATION PARAMETERS OF DEIONIZED WATER AT 22 °C USING THE PROPOSED HYBRID METHOD COMPARED WITH THE LITERATURE DATA [16]–[18], [44]

Debye parameters	Measurement frequency (GHz)	Method	ϵ_∞	$\Delta\epsilon_1$	τ_1 (ps)	$\Delta\epsilon_2$	τ_2 (ps)
This work	1 - 110	CPW microfluidics	4.50±0.42	72.34±0.85	8.59±0.11	2.12±0.27	1.36±0.65
Ellison [44]	1 - 500	Combination of methods	4.49	72.22	9.25	2.75	1.23
Buchner *et al.* [18]	0.2 - 410	Waveguide interferometer, time-domain reflectometer, *etc.*	4.48	73.06	9.11	1.97	1.16
Kaatze [16]	1.1 - 57	Travelling-wave technique	5.44±0.2	74.03±0.28	8.92±0.05	-	-
Peacock [17] (24.5±1.2°C)	75 - 100	Free-space	4.13±0.13	72.39±0.62	8.41±0.04	1.66±0.60	0.93±0.14

The extracted water relative permittivity obtained with the hybrid method $\epsilon_{r,H_2O,\text{hybrid}}$ was fit to a double Debye model that is capable of describing two dielectric relaxations. The double Debye model is necessary for describing water permittivity to 110 GHz, because pure water at room temperature has two relaxations around 20 and 130 GHz [44]. The first relaxation is due to the partial orientations of permanent water dipoles [3], while for the second relaxation, accepted interpretation is still lacking in the literature [18]. The double Debye model is as follows:

$$\epsilon_r = \epsilon_\infty + \frac{\Delta\epsilon_1}{1 + j\omega\tau_1} + \frac{\Delta\epsilon_2}{1 + j\omega\tau_2} \tag{8}$$

where ϵ_r is the complex material relative permittivity, and ϵ_∞ is the relative permittivity at infinitely high frequencies. The parameters $\Delta\epsilon_1$ and τ_1 represent the dielectric relaxation strength and the time constant of the first relaxation, and $\Delta\epsilon_2$ and τ_2 represent the dielectric relaxation strength and the time constant of the second relaxation.

Fig. 4(c) and (d) shows the real and imaginary parts of $\epsilon_{r,\text{H}_2\text{O},\text{hybrid}}$ and its fitting to the double Debye model in (8) $\epsilon_{r,\text{H}_2\text{O},\text{hybrid,double Debye}}$. During the double Debye fitting, in order to avoid overweighting in the low frequency region of the permittivity data, the fitting was performed with a linear frequency scale. For this purpose, the frequency points used for the fitting were "subsampled" from the original log sweep, starting from the highest frequency point. As is clear from Fig. 4(c) and (d), the double Debye model has a very small fit residual. However, in the sub-GHz region of Fig. 4(d), the actual measurement uncertainties in $\epsilon''_{r,\text{H}_2\text{O},\text{hybrid}}$ are larger than the calculated values in Fig. 4(b). The uncertainties that were not taken into account might be caused by the VNA noise.

In order to assess the quality of the fit, Fig. 4(e) and (f) shows the fitting residuals for three cases together with the uncertainties of the complex relative permittivity from the hybrid method $u(\epsilon_{r,\text{H}_2\text{O},\text{hybrid}})$. The first case was when the double Debye fitting was applied to the complex relative permittivity from the hybrid method (circles). In this case, the residuals are below $u(\epsilon_{r,\text{H}_2\text{O},\text{hybrid}})$ for most of the frequency points, which indicates the success of the fitting.

The two other cases are shown for comparison purposes: when the fitting model was only single Debye and the data were from the hybrid method (triangles), and when the fitting model was double Debye but the fitting data were from the least-squares optimization algorithm (squares). In both cases, the fit residuals are higher at frequencies above 50 GHz than the first case. The reason for the higher residuals of the first case is that the single Debye model is unable to model water relaxation far beyond its first relaxation frequency around 20 GHz. The reason for the second case is that the measurement uncertainties in the least-squares optimization algorithm were higher than the other algorithms at frequencies above 50 GHz, and these uncertainties could not be modeled by changes in the Debye relaxation parameters.

Fig. 4(g) and (h) compares the difference between the measured water relative permittivity and the literature values [44] $|\epsilon_{r,\text{H}_2\text{O},\text{hybrid}} - \epsilon_{\text{r},\text{H}_2\text{O},\text{literature}}|$ (circles) with the measurement uncertainties of the hybrid method. We found that above 60 GHz, there is an excellent match between the measured and literature values of the real part of water relative permittivity. The differences in this region are around 1%. However, the differences are larger for frequencies around 30 GHz for the real part and for the frequencies above 30 GHz for the imaginary part, with the maximum value being around 6%. The source of this discrepancy is the subject of future work. The dotted line shows that the uncertainties of the double Debye-fit water relative permittivity $u(\epsilon_{r,\text{H}_2\text{O},\text{hybrid,double Debye}})$ follow $u(\epsilon_{r,\text{H}_2\text{O},\text{hybrid}})$, which means that by using the hybrid method, the double Debye model was able to capture the error mechanisms discussed previously in Section IV-A.

Table III lists the double Debye model parameters for the measured water relative permittivity obtained with the hybrid method. Our measured double Debye model parameters agree with the literature values, except for the first relaxation time constant, τ_1. The relatively large discrepancy in τ_1 is related with the permittivity discrepancy around the first water relaxation frequency shown in Fig. 4(g) and (h). The reason for the relatively large uncertainties in the relaxation parameters of the second water relaxation is likely due to the range of the data, which only catches the very beginning of the second water relaxation around 130 GHz. Another reason may be due to the size of the relaxation, which is small compared with its lower frequency counterpart. Hence, we suppose that further increase of the measurement frequency will increase the accuracy when characterizing the second relaxation of water.

VI. UNCERTAINTY ANALYSIS FOR THE EXTRACTED WATER RELATIVE PERMITTIVITY FROM THE THREE ALGORITHMS

We found that the hybrid method was able to successfully reduce the uncertainty and improve the accuracy in the

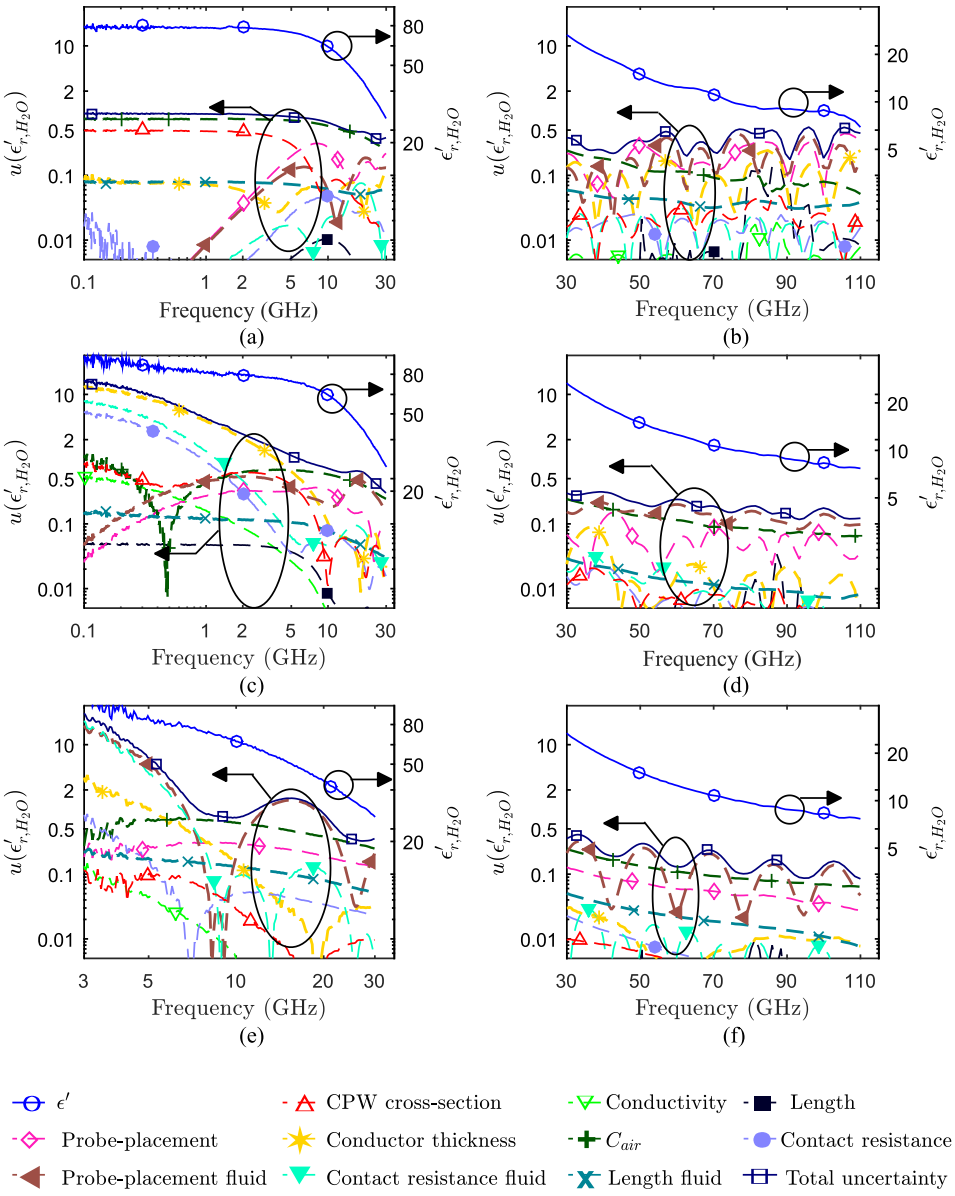

Fig. 5. Breakdown of uncertainties in $\epsilon'_{r,\mathrm{H_2O}}$ extraction for (a) and (b) least-squares optimization-based method, (c) and (d) closed-form equation method, and (e) and (f) trace method. The error mechanisms from the microfluidic channel have "fluid" in the legend names, and other mechanisms are from the on-wafer MTRL calibration.

complex permittivity of water by effectively choosing the method with the lowest uncertainty. Here, the uncertainties of the different algorithms are studied in more detail. Fig. 5 shows the breakdown of the standard uncertainties of the real part of measured water relative permittivity obtained with the three extraction algorithms $u(\epsilon_{r,\mathrm{H_2O}})$. The dc 30-GHz part of the uncertainty breakdown is shown on the left column and the 30–110-GHz part is shown on the right column.

We found that at low frequencies, the least-squares optimization algorithm is least sensitive to the error mechanisms considered in the uncertainty analysis, and gives nearly constant relative permittivity values below 2 GHz. At low frequencies, the values from the closed-form equation and the trace algorithm show obvious deviations from the least-squares optimization algorithm. The closed-form equation and the trace algorithm are based on propagation constant measurement only (4) and (5), which explains why they are inaccurate at low frequencies. While the least-squares optimization algorithm optimizes for the minimum difference in all the four S-parameters, which means that it uses both the propagation constant and the characteristic impedance. At low frequencies, errors from the propagation constant and the characteristic impedance cancel out, so the least-squares optimization algorithm is less sensitive to error mechanisms than the other two algorithms.

However, in the millimeter wave frequency range, the least-squares optimization algorithm becomes increasingly sensitive to probe-placement errors, both from the MTRL calibration

(diamonds) and from the microfluidic channel measurement (left-pointing triangles). In contrast, the closed-form equation algorithm and the trace algorithm become less sensitive to probe-placement errors as frequency increases. A possible explanation is that at high frequencies, the propagation constant measurement becomes more accurate, and the characteristic impedance measurement becomes more sensitive. In order to achieve accurate measurement of water permittivity over a wider bandwidth, the hybrid method used the least-squares optimization algorithm at low frequencies, and avoided its high uncertainties at high frequencies by the use of the closed-form equation algorithm or the trace algorithm.

VII. Conclusion

In this paper, we have presented a hybrid method for accurate measurements of dielectric fluids permittivity using a single CPW microfluidic device. The hybrid method is based on three permittivity extraction algorithms and an uncertainty analysis based on the NIST Microwave Uncertainty Framework. The validity of the hybrid method has been demonstrated by measurements of deionized water at 22 °C. Since the permittivity of biological fluids is close to that of water, the proposed method will apply to any biological fluids. Also, we proposed and validated a new method for characterizing the material used to make the microfluidic channel using a single microfluidic device. The advantage of this method is that it does not require extra deembedding structures.

Acknowledgment

The authors would like to thank Dr. M. Wallis for the technical support, Dr. G. Avolio for the scientific discussions, and Dr. R. A. Chamberlin, Dr. C. J. Long, Dr. D. Gu, and Dr. C. M. Weil for reviewing this paper.

References

[1] T. Sato and R. Buchner, "Cooperative and molecular dynamics of alcohol/water mixtures: The view of dielectric spectroscopy," *J. Mol. Liq.*, vol. 117, nos. 1–3, pp. 23–31, Mar. 2005.

[2] T. H. Basey-Fisher *et al.*, "Microwave debye relaxation analysis of dissolved proteins: Towards free-solution biosensing," *Appl. Phys. Lett.*, vol. 99, no. 23, pp. 233703-1–233703-3, Dec. 2011.

[3] C. Polk and E. Postow, *Handbook of Biological Effects of Electromagnetic Fields*, 2nd ed. Boca Raton, FL, USA: CRC Press, 1996.

[4] C. Cametti, S. Marchetti, C. M. C. Gambi, and G. Onori, "Dielectric relaxation spectroscopy of lysozyme aqueous solutions: analysis of the δ-dispersion and the contribution of the hydration water," *J. Phys. Chem. B*, vol. 115, no. 21, pp. 7144–7153, Jun. 2011.

[5] N. Q. Vinh, S. J. Allen, and K. W. Plaxco, "Dielectric spectroscopy of proteins as a quantitative experimental test of computational models of their low-frequency harmonic motions," *J. Amer. Chem. Soc.*, vol. 133, no. 23, pp. 8942–8947, Jun. 2011.

[6] H. P. Schwan and K. R. Foster, "RF-field interactions with biological systems: Electrical properties and biophysical mechanisms," *Proc. IEEE*, vol. 68, no. 1, pp. 104–113, Jan. 1980.

[7] M. Wolf, R. Gulich, P. Lunkenheimer, and A. Loidl, "Broadband dielectric spectroscopy on human blood," *Biochim. Biophysica Acta-Gen. Subjects*, vol. 1810, no. 8, pp. 727–740, Aug. 2011.

[8] K. Grenier *et al.*, "Integrated broadband microwave and microfluidic sensor dedicated to bioengineering," *IEEE Trans. Microw. Theory Techn.*, vol. 57, no. 12, pp. 3246–3253, Dec. 2009.

[9] F. Artis, D. Dubuc, J.-J. Fournie, M. Poupot, and K. Grenier, "Microwave dielectric spectroscopy of cell membrane permeabilization with saponin on human b lymphoma cells," in *IEEE MTT-S Int. Microw. Symp. Dig.*, Jun. 2014, pp. 1–4.

[10] J. C. Booth, N. D. Orloff, J. Mateu, M. Janezic, M. Rinehart, and J. A. Beall, "Quantitative permittivity measurements of nanoliter liquid volumes in microfluidic channels to 40 GHz," *IEEE Trans. Instrum. Meas.*, vol. 59, no. 12, pp. 3279–3288, Dec. 2010.

[11] T. Chen, F. Artis, D. Dubuc, J.-J. Fournie, M. Poupot, and K. Grenier, "Microwave biosensor dedicated to the dielectric spectroscopy of a single alive biological cell in its culture medium," in *IEEE MTT-S Int. Microw. Symp. Dig.*, Jun. 2013, pp. 1–4.

[12] Y. Ning *et al.*, "Broadband electrical detection of individual biological cells," *IEEE Trans. Microw. Theory Techn.*, vol. 62, no. 9, pp. 1905–1911, Sep. 2014.

[13] A. Raj, W. S. Holmes, and S. R. Judah, "Wide bandwidth measurement of complex permittivity of liquids using coplanar lines," *IEEE Trans. Instrum. Meas.*, vol. 50, no. 4, pp. 905–909, Aug. 2001.

[14] S. Seo, T. Stintzing, I. Block, D. Pavlidis, M. Rieke, and P. G. Layer, "High frequency wideband permittivity measurements of biological substances using coplanar waveguides and application to cell suspensions," in *IEEE MTT-S Int. Microw. Symp. Dig.*, Jun. 2008, pp. 915–918.

[15] S. Liu, I. Ocket, M. Cauwe, D. Schreurs, and B. Nauwelaers, "Sensitivity analysis of broadband on-wafer dielectric spectroscopy of yeast cell suspensions up to 110 GHz," *IEEE Microw. Wireless Compon. Lett.*, vol. 25, no. 3, pp. 199–201, Mar. 2015.

[16] U. Kaatze, "Complex permittivity of water as a function of frequency and temperature," *J. Chem. Eng. Data*, vol. 34, no. 4, pp. 371–374, Oct. 1989.

[17] J. R. Peacock, "Millimetre wave permittivity of water near 25°," *J. Phys. D, Appl. Phys.*, vol. 42, no. 20, pp. 205501-1–205501-6, Sep. 2009.

[18] R. Buchner, J. Barthel, and J. Stauber, "The dielectric relaxation of water between 0° and 35°," *Chem. Phys. Lett.*, vol. 306, no. 1, pp. 57–63, Jun. 1999.

[19] U. Kaatze, "Reference liquids for the calibration of dielectric sensors and measurement instruments," *Meas. Sci. Technol.*, vol. 18, no. 4, pp. 967–976, Feb. 2007.

[20] E. Ermilova, F. F. Bier, and R. Hölzel, "Dielectric measurements of aqueous DNA solutions up to 110 GHz," *Phys. Chem. Chem. Phys.*, vol. 16, no. 23, pp. 11256–11264, Apr. 2014.

[21] G. M. Whitesides, "The origins and the future of microfluidics," *Nature*, vol. 442, no. 27, pp. 368–373, Jul. 2006.

[22] D. Mark, S. Haeberle, G. Roth, F. von Stetten, and R. Zengerle, "Microfluidic lab-on-a-chip platforms: Requirements, characteristics and applications," *Chem. Soc. Rev.*, vol. 39, no. 3, pp. 1153–1182, Mar. 2010.

[23] N. Meyne, W. Müller-Wichards, H. K. Trieu, and A. F. Jacob, "Quasi-lumped coplanar transmission-line sensors for broadband liquid characterization," in *Proc. Eur. Microw. Conf.*, 2014, pp. 687–690.

[24] N. Meyne, S. Latus, and A. F. Jacob, "Corrugated coplanar transmission-line sensor for broadband liquid sample characterization," in *Proc. German Microw. Conf.*, 2014, pp. 1–4.

[25] S. Liu *et al.*, "Broadband dielectric spectroscopy calibration using calibration liquids with unknown permittivity," in *Proc. 84th ARFTG Microw. Meas. Conf.*, 2014, pp. 1–5.

[26] D. Williams, "NIST uncertainty framework software package," RF Technol. Division, Commun. Technol. Lab., Nat. Inst. Standards Technol. (NIST), Boulder, CO, USA, 2017.

[27] N. J. Farcich, J. Salonen, and P. M. Asbeck, "Single-length method used to determine the dielectric constant of polydimethylsiloxane," *IEEE Trans. Microw. Theory Techn.*, vol. 56, no. 12, pp. 2963–2971, Dec. 2008.

[28] *Evaluation of Measurement Data-Guide to the Expression of Uncertainty in Measurement (GUM)*, Joint Committee Guides Metrol., 2008.

[29] R. B. Marks, "A multiline method of network analyzer calibration," *IEEE Trans. Microw. Theory Techn.*, vol. 39, no. 7, pp. 1205–1215, Jul. 1991.

[30] R. B. Marks and D. F. Williams, "Characteristic impedance determination using propagation constant measurement," *IEEE Microw. Guided Wave Lett.*, vol. 1, no. 6, pp. 141–143, Jun. 1991.

[31] D. F. Williams and R. B. Marks, "Transmission line capacitance measurement," *IEEE Microw. Guided Wave Lett.*, vol. 1, no. 9, pp. 243–245, Sep. 1991.

[32] D. M. Pozar, *Microwave engineering*. Reading, MA, USA: Addison-Wesley, 1990.

[33] R. B. Marks, "Formulations of the basic vector network analyzer error model including switch-terms," in *Proc. 50th ARFTG Microw. Meas. Conf.*, vol. 32. 1997, pp. 115–126.

[34] M. D. Janezic and J. A. Jargon, "Complex permittivity determination from propagation constant measurements," *IEEE Microw. Guided Wave Lett.*, vol. 9, no. 2, pp. 76–78, Feb. 1999.

[35] I. Huygen, C. Steukers, and F. Duhamel, "A wideband line-line dielectrometric method for liquids, soils, and planar substrates," *IEEE Trans. Instrum. Meas.*, vol. 50, no. 5, pp. 1343–1348, Oct. 2001.
[36] J. Liu *et al.*, "Process research of high aspect ratio microstructure using SU-8 resist," *Microsyst. Technol.*, vol. 10, no. 4, pp. 265–268, May 2004.
[37] S. D. Minteer, Ed., *Microfluidic Techniques: Reviews and Protocols*. New York, NY, USA: Humana Press, 2006.
[38] N. D. Orloff *et al.*, "A compact variable-temperature broadband series-resistor calibration," *IEEE Trans. Microw. Theory Techn.*, vol. 59, no. 1, pp. 188–195, Jan. 2011.
[39] J. M. Dewdney and J. Wang, "Characterization the microwave properties of SU-8 based on microstrip ring resonator," in *Proc. WAMICON*, 2009, pp. 1–5.
[40] A. Ghannam, C. Viallon, D. Bourrier, and T. Parra, "Dielectric microwave characterization of the SU-8 thick resin used in an above IC process," in *Proc. Eur. Microw. Conf.*, 2009, pp. 1041–1044.
[41] N. Ghalichechian and K. Sertel, "Permittivity and loss characterization of SU-8 films for mmW and terahertz applications," *IEEE Antennas Wireless Propag. Lett.*, vol. 14, pp. 723–726, Dec. 2014.
[42] R. G. Pierce, R. Islam, R. M. Henderson, and A. Blanchard, "SU-8 2000 millimeter wave material characterization," *IEEE Microw. Wireless Compon. Lett.*, vol. 24, no. 6, pp. 427–429, Jun. 2014.
[43] J. C. Booth, J. Mateu, M. Janezic, J. Baker-Jarvis, and J. A. Beall, "Broadband permittivity measurements of liquid and biological samples using microfluidic channels," in *IEEE MTT-S Int. Microw. Symp. Dig.*, Jun. 2006, pp. 1750–1753.
[44] W. J. Ellison, "Permittivity of pure water, at standard atmospheric pressure, over the frequency range 0–25 THz and the temperature range 0–100 °C," *J. Phys. Chem. Ref. Data*, vol. 36, no. 1, pp. 1–18, Feb. 2007.

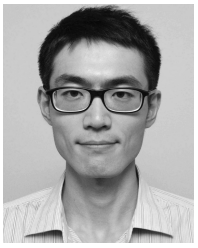

Song Liu received the Ph.D. degree in electrical engineering from KU Leuven, Leuven, Belgium, in 2016.

In 2014 and 2015, he spent six months with the RF Technology Division, National Institute of Standards and Technology (NIST), Boulder, CO, USA, under the support of KU Leuven. His current research interests include RF power amplifier design, microwave biomedical applications, vector network analyzer calibration, and material characterization.

Dr. Liu was one of the recipient of the Automatic RF Techniques Group Roger Pollard Student Fellowship in 2013 and the IEEE Microwave Theory and Techniques Society Graduate Fellowship in 2014.

Nathan D. Orloff, photograph and biography not available at the time of publication.

Charles (Cully) A. E. Little received the B.S. degree in physics from Appalachian State University, Boone, NC, USA, in 2008, and the M.S. degree from the Mechanical Engineering Department, University of Colorado, Boulder, CO, USA, in 2013, where he is currently pursuing the Ph.D. degree in mechanical engineering.

He was a Research Assistant with Duke University, Durham, NC, USA, as part of the Neutrino Group, Physics Department. He was with the National Institute of Standards and Technology (NIST), Boulder, CO, USA, since beginning his master's work in 2010, developing fabrication techniques for microfluidics. His current research interests include integrated microfluidic/microwave devices for measuring the electrical and magnetic properties of fluids.

Wei Zhao received the B.S. and M.S. degrees in measurement science and instruments from Xidian University, Xi'an, China, in 2005 and 2008, respectively, and the Ph.D. degree in communication and information system from the Nanjing University of Aeronautics and Astronautics, Nanjing, China, in 2011.

He joined Xidian University in 2011, where he is currently a Lecturer with the School of Electro-Mechanical Engineering. In 2014, he was a Guest Researcher with the National Institute of Standards and Technology (NIST), Boulder, CO, USA, where he spent one year on the development of the uncertainty analysis and on-wafer vector network analyzer measurements.

James C. Booth, photograph and biography not available at the time of publication.

Dylan F. Williams (M'80–SM'90–F'02) received the Ph.D. degree in electrical engineering from the University of California at Berkeley, Berkeley, CA, USA, in 1986.

He joined the Electromagnetic Fields Division, National Institute of Standards and Technology (NIST), Boulder, CO, USA, in 1989, where he develops electrical waveform and microwave metrology. He has authored over 100 technical papers.

Dr. Williams was a recipient of the Department of Commerce Bronze and Silver Medals, the Astin Measurement Science Award, two Electrical Engineering Laboratory's Outstanding Paper Awards, three Automatic RF Techniques Group (ARFTG) Best Paper Awards, the ARFTG Automated Measurements Technology Award, the IEEE Morris E. Leeds Award, the European Microwave Prize, and the 2013 IEEE Joseph F. Keithley Award. He is currently the President of the IEEE Microwave Theory and Techniques Society. He served as an Editor-in-Chief of the IEEE TRANSACTIONS ON MICROWAVE THEORY AND TECHNIQUES from 2006 to 2010 and as the Executive Editor of the IEEE TRANSACTIONS ON TERAHERTZ SCIENCE AND TECHNOLOGY.

Ilja Ocket (M'09) received the M.Sc. and Ph.D. degrees in electrical engineering from KU Leuven, Leuven, Belgium, in 1998 and 2009, respectively.

He has been with imec, Leuven, and KU Leuven, since 1999. With imec, he is currently involved in millimeter-wave antenna modules and packaging for 79- and 140-GHz radar. With KU Leuven, he leads the group working in the area of microwave and millimeter-wave applications for biology and medicine, and is also involved in integrated couplers for (sub)millimeter plastic waveguides.

Dominique M. M.-P. Schreurs (S'90–M'97–SM'02–F'12) received the M.Sc. degree in electronic engineering and Ph.D. degree from KU Leuven, Leuven, Belgium.

She has been a Visiting Scientist with Agilent Technologies, ETH Zurich, Zurich, Switzerland, and the National Institute of Standards and Technology (NIST), Boulder, CO, USA. She is currently a Full Professor with KU Leuven. Her current research interests include microwave and millimeter-wave characterization and modeling of active devices and bioliquids, and system design for wireless telecommunications and biomedical applications.

Dr. Schreurs was the Co-Chair of the European Microwave Conference in 2008. She is serving on the AdCom of the IEEE Microwave Theory and Techniques Society (MTT-S). She is the Chair of the MTT-S Meetings and Symposia Committee, a past MTT-S Distinguished Microwave Lecturer, and the past Editor-in-Chief of the IEEE TRANSACTIONS ON MICROWAVE THEORY AND TECHNIQUES. She serves as the Vice President on the Executive Committee of the Automatic RF Techniques Group (ARFTG) Organization and the General Chair of the 2007, 2012, and 2018 Spring ARFTG Conference.

Bart Nauwelaers (S'80–M'86–SM'99), photograph and biography not available at the time of publication.